JGR Biogeosciences

RESEARCH ARTICLE
10.1029/2020JG005680

Bullet-Shaped Magnetite Biomineralization Within a Magnetotactic Deltaproteobacterium: Implications for Magnetofossil Identification

Jinhua Li[1,2,3], Nicolas Menguy[3,4], Andrew P. Roberts[5], Lin Gu[6], Eric Leroy[7], Julie Bourgon[7], Xin'an Yang[6], Xiang Zhao[5], Peiyu Liu[1,2,3,8], Hitesh G. Changela[1], and Yongxin Pan[1,3,8]

[1]Key Laboratory of Earth and Planetary Physics, Institute of Geology and Geophysics, Innovation Academy for Earth Sciences, Chinese Academy of Sciences, Beijing, China, [2]Laboratory for Marine Geology, Qingdao National Laboratory for Marine Science and Technology, Qingdao, China, [3]International Associated Laboratory of Evolution and Development of Magnetotactic Multicellular Organisms (LIA-MagMC), CNRS-CAS, Beijing, China, [4]IMPMC, Sorbonne Universités, Paris, France, [5]Research School of Earth Sciences, Australian National University, Canberra, ACT, Australia, [6]Beijing National Laboratory for Condensed Matter Physics, Institute of Physics, Chinese Academy of Sciences, Beijing, China, [7]ICMPE, University Paris East, Thiais, France, [8]College of Earth Sciences, University of Chinese Academy of Sciences, Beijing, China

Key Points:
- Magnetite produced by MTB carries stable paleomagnetic signals, but paleoenvironmental interpretation of biogenic magnetite is less obvious
- We find that magnetite crystals grow by a multistep process in a novel MTB to form highly elongated, bullet-shaped magnetite
- Species-specific magnetite biomineralization indicates that magnetite morphology is a proxy for ancient MTB taxonomic groups or species

Supporting Information:
- Supporting Information S1
- Movie S1
- Movie S2

Correspondence to:
J. H. Li,
lijinhua@mail.iggcas.ac.cn

Citation:
Li, J., Menguy, N., Roberts, A. P., Gu, L., Leroy, E., Bourgon, J., et al. (2020). Bullet-shaped magnetite biomineralization within a magnetotactic Deltaproteobacterium: Implications for magnetofossil identification. *Journal of Geophysical Research: Biogeosciences*, *125*, e2020JG005680. https://doi.org/10.1029/2020JG005680

Received 6 FEB 2020
Accepted 16 JUN 2020
Accepted article online 30 JUN 2020

Abstract Magnetite produced by magnetotactic bacteria (MTB) provides stable paleomagnetic signals because it occurs as natural single-domain magnetic nanocrystals. MTB can also provide useful paleoenvironmental information because their crystal morphologies are associated with particular bacterial groups and the environments in which they live. However, identification of the fossil remains of MTB (i.e., magnetofossils) from ancient sediments or rocks is challenging because of their generally small sizes and because the growth, morphology, and chain assembly of magnetite within MTB are not well understood. Nanoscale characterization is, therefore, needed to understand magnetite biomineralization and to develop magnetofossils as biogeochemical proxies for paleoenvironmental reconstructions. Using advanced transmission electron microscopy, we investigated magnetite growth and chain arrangements within magnetotactic Deltaproteobacteria strain WYHR-1, which reveals how the magnetite grows to form elongated, bullet-shaped nanocrystals. Three crystal growth stages are recognized: (i) initial isotropic growth to produce nearly round ~20 nm particles, (ii) subsequent anisotropic growth along the [001] crystallographic direction to ~75 nm lengths and ~30–40 nm widths, and (iii) unidirectional growth along the [001] direction to ~180 nm lengths, with some growing to ~280 nm. Crystal growth and habit differ from that of magnetite produced by other known MTB strains, which indicates species-specific biomineralization. These findings suggest that magnetite biomineralization might be much more diverse among MTB than previously thought. When characterized adequately at species level, magnetofossil crystallography, and apomorphic features are, therefore, likely to become useful proxies for ancient MTB taxonomic groups or species and for interpreting the environments in which they lived.

Plain Language Summary Biomineralization is a widespread process that provides living organisms with mineralized skeletons and organelles. Biominerals are mainly responsible for Earth's fossil record. As a striking example of microbial biomineralization, magnetotactic bacteria form intracellular chains of magnetic nanocrystals that they use to sense Earth's magnetic field. Their fossilized remains (magnetofossils) are being used increasingly to reconstruct paleomagnetic and paleoenvironmental information. However, magnetofossil identification remains challenging because magnetite particle growth and chain assembly processes are poorly understood. We report a species-specific crystal growth and chain arrangement process in a novel magnetotactic strain WYHR-1. Our findings suggest that magnetofossil crystallography could become a proxy for ancient bacterial taxonomic groups or species and for interpreting the environments in which they lived.

1. Introduction

Magnetotactic bacteria (MTB) are remarkable organisms that can biomineralize and sense Earth's magnetic field. Through biologically controlled mineralization (BCM), they form intracellular nanometer-sized,

magnetically ideal single-domain (SD) crystals of magnetite (Fe_3O_4) and/or greigite (Fe_3S_4), which are each enveloped by a lipid bilayer membrane called a magnetosome (Uebe & Schüler, 2016). Magnetosomes are generally organized into a fixed chain or chains, which serve as an intracellular biocompass that causes MTB to swim along Earth's magnetic field lines in aquatic environments. This phenomenon is known as magnetotaxis (Bazylinski & Frankel, 2004). Fossil remains of MTB called magnetofossils have been found widely in Cenozoic sediments (Roberts et al., 2012) and have even been identified in pre-Cambrian rocks (Kopp & Kirschvink, 2008). Magnetosomal magnetite has distinctive physical, chemical, crystallographic, and magnetic properties that contrast with those of detrital and other types of magnetite (Amor et al., 2015; Kopp & Kirschvink, 2008; Li, Benzerara, et al., 2013; Moskowitz et al., 1993), which make magnetofossils important and ideal carriers of paleomagnetic and paleoenvironmental signals (Chang et al., 2018; Larrasoaña et al., 2014; Roberts et al., 2011; Usui et al., 2017; Yamazaki et al., 2019).

In nature, MTB are morphologically, phylogenetically, and physiologically diverse. They have been found in all continents and are ubiquitous in freshwater, brackish, marine, and hypersaline habitats, where they occur predominantly at or just below the oxic-anoxic interface (OAI) (Lefèvre & Bazylinski, 2013). Phylogenetically, they are scattered within various phyla, such as the Alphaproteobacteria, Deltaproteobacteria, and Gammaproteobacteria classes of the Proteobacteria phylum; the Nitrospirae phylum, the "Candidatus Omnitrophica phylum" (Kolinko et al., 2016; Lefèvre & Bazylinski, 2013), and probably the candidate phylum Latescibacteria, and the classes Zetaproteobacteria and "Candidatus Lambdaproteobacteria" (Lin et al., 2018). It has been shown that the distribution of MTB communities correlates with environmental factors such as salinity, chemical composition, redox potential, and even magnetic field strength (Lin, Bazylinski, et al., 2014). Consistent with the phylogenetic and physiological diversity of MTB, magnetosomes also have diverse crystal morphologies and compositions (Pósfai, Lefèvre, et al., 2013). For instance, magnetotactic Alphaproteobacteria and Gammaproteobacteria biomineralize octahedral, cubo-octahedral, or elongated-prismatic crystals of magnetite, while MTB in the phyla Nitrospirae and Omnitrophica produce bullet-shaped magnetite crystals (Araujo et al., 2016; Kolinko et al., 2016; Li, Ge, et al., 2013; Li et al., 2017; Meldrum et al., 1993a; Sparks et al., 1990; Zhang et al., 2017). Magnetotactic Deltaproteobacteria synthesize either magnetite-type or greigite-type crystals, or both within a single cell (Lefèvre & Bazylinski, 2013). Bullet-shaped magnetite is generally produced by most magnetotactic Deltaproteobacteria (Lefèvre, Menguy, et al., 2011; Lefèvre, Pósfai, et al., 2011; Li et al., 2019; Pósfai et al., 2006; Zhou et al., 2012), although so-called parallelepipedal magnetite has been observed in *Candidatus* Magnetoglobus multicellularis (Abreu et al., 2013) and in *Candidatus* Magnetananas rongchenensis (Chen et al., 2015). Likewise, the greigite within magnetotactic Deltaproteobacteria is morphologically diverse and includes cubo-octahedral, elongated-prismatic, bullet-shaped, and pleomorphic shapes (Lefèvre & Bazylinski, 2013). Recently, Lin et al. (2017) performed metagenomic and phylogenetic analyses of uncultured MTB and demonstrated that MTB might have originated before or near the Archean Eon. Magnetite and greigite biomineralization in the Bacterial domain might have a common ancient origin that followed different evolutionary and taxonomic routes (Lin et al., 2017, 2018). Magnetofossils, therefore, have great potential for constraining the (1) origin and evolution of iron-based (Fe_3O_4 and Fe_3S_4) biomineralization and magnetotaxis within MTB, (2) environmental conditions in which MTB lived, and (3) development of proxies for identifying bacterial taxonomic groups, strains, and species of ancient MTB.

The use of magnetic and biogeochemical proxy information recorded by magnetofossils depends on understanding the bacterial diversity of MTB and how biomineralization relates to this diversity within environments. Due to the adaptation to complex chemical gradients in stratified environments, only a few MTB species have been isolated in axenic culture. Most cultured strains belong to the Alphaproteobacteria class beside several Deltaproteobacteria and Gammaproteobacteria strains. In the past decade, significant progress has been made in identifying MTB from natural environments using culture-independent analysis methods at the single-cell level (Kolinko et al., 2012; Li et al., 2017). For instance, by coupling fluorescence in situ hybridization (FISH) analysis with transmission or scanning electron microscope (TEM or SEM) observation, a so-called coupled FISH-SEM or FISH-TEM approach, MTB cells from natural environments can be identified phylogenetically and structurally at the single-cell level (Koziaeva et al., 2019; Li et al., 2017, 2019; Qian et al., 2019, 2020; Zhang et al., 2017). On the other hand, rapid development of metagenomics and single-cell genomics has enabled identification of more magnetosome gene clusters (MGCs) responsible for magnetosome biomineralization in uncultured MTB (Jogler et al., 2011; Kolinko

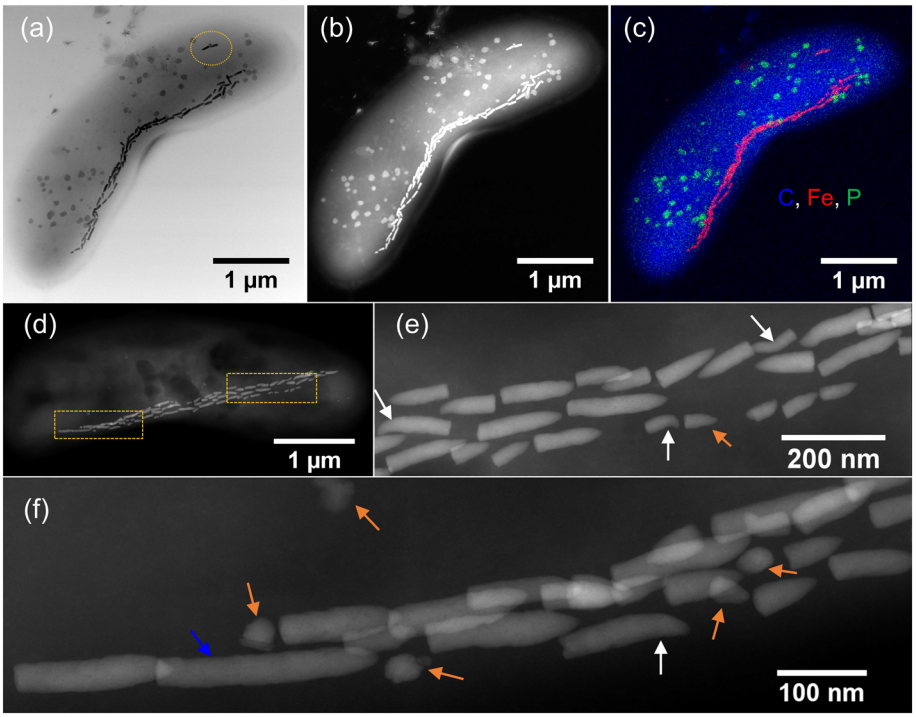

Figure 1. Morphology, chemistry, and assemblage of WYHR-1 magnetosomal magnetite analyzed by atomic resolution HAADF-STEM. (a) Bright field TEM image, (b) HAADF-STEM image, and (c) chemical composition map of a WYHR-1 cell. In (c), C-, P-, and Fe-Kα distributions are indicated in blue, green, and red, respectively. (d) HAADF-STEM image of a WYHR-1 cell. (e–f) Close-up images of WYHR-1 magnetosomes as indicated by the yellow dashed boxes in Figure 1d. Magnetosomes away from the straight bundle are indicated by yellow dashed circles in Figure 1a. Kinked, small, and long (>200 nm) magnetosomes are indicated by white, yellow, and blue arrows in Figures 1e–1f, respectively.

et al., 2014, 2016; Lin et al., 2018). These pioneering studies pave the way to better understand phylogenetic diversity and to predict the genomic sequences responsible for magnetosome biomineralization within MTB. However, systematic studies of crystal growth and chain assembly of magnetosomal biominerals particularly within MTB outside the Alphaproteobacteria class remain sparse. Such gaps between bacterial phylogenetics and magnetosomal mineralogy hamper the comprehensive understanding of biomineralization and the use of magnetofossils in paleomagnetic and paleoenvironmental reconstructions.

We focus here on bullet-shaped magnetite mainly because it is thought to be (1) the first and oldest crystal type biomineralized by ancient MTB (Lefèvre, Trubitsyn, Abreu, Kolinko, de Almeida, & de Vasconcelos, 2013; Lin et al., 2017), (2) the geologically best preserved magnetofossil type (Lefèvre, Pósfai, et al., 2011; Li et al., 2015, 2010; Mann et al., 1987), and (3) a sensitive proxy for reduced environmental oxygen (Mao et al., 2014; Yamazaki et al., 2019). Moreover, compared to magnetotactic Nitrospirae (Li et al., 2010, 2015), crystal growth and chain assembly of bullet-shaped magnetite within the magnetotactic Deltaproteobacteria have not been studied systematically. *Candidatus* Magnetcampylobacter weiyangensis strain WYHR-1, which was identified recently from Weiyang Lake, Xi'an, China (Li et al., 2019), represents a novel genus from the Deltaproteobacteria class of the Proteobacteria phylum. It has a large bean-shaped cell that contains dozens of bullet-shaped magnetosomes and many polyphosphate inclusions (Figures 1 and S1). In contrast to the kinked morphologies of bullet-shaped magnetite produced by the magnetotactic Nitrospirae (Li et al., 2010, 2015) the magnetite produced by WYHR-1 is generally straight and highly elongated (Li et al., 2019). Crystals are organized into a single straight bundle along the cell long axis, with occasionally a few particles located away from the bundle (Figure 1). Using various advanced TEM analyses down to atomic scales, we study here the multistep pattern of magnetosomal crystal growth for WYHR-1 and explore the implications of this species-specific crystal growth and morphology in relation to developing magnetite morphology as a proxy for ancient MTB taxonomic units and for interpreting the environments in which they lived.

2. Materials and Methods

2.1. Sample Preparation

Intact WYHR-1 cells were prepared for various TEM analyses as described by Li et al. (2019). Briefly, WYHR-1 cells were separated magnetically from Weiyang Lake sediments using a modified magnetic separation apparatus for ~1 hr. The collected WYHR-1 cells were washed three times in Milli-Q water and were deposited onto the surface of carbon-coated TEM grids. All TEM grid samples were stored in a pure N_2 atmosphere at −20°C prior to TEM observations.

2.2. TEM and HRTEM Imaging

TEM experiments were performed on a JEOL JEM-2100F microscope at 200 kV. This instrument is equipped with a field emission gun and an ultra-high resolution (UHR) pole piece that is capable of providing high spatial resolution lattice imaging and microstructure analysis. Crystal lengths and widths were measured from high-resolution TEM (HRTEM) images of individual magnetite particles along their long axis and maximum width perpendicular to the long axis, respectively. Crystal habits were determined by combined Fourier analysis of HRTEM images for individual particles and crystallographic investigations (Faivre et al., 2008; Li et al., 2015). Idealized magnetosome shapes were modeled with the KrystalShaper software package (JCrystalSoft).

2.3. TEM Tomography and Crystal Orientation Mapping

In order to ascertain the exact morphology of WYHR-1 magnetosomes, TEM tomography was performed in the Scanning TEM (STEM) and High Angle Annular Dark Field (HAADF) imaging mode on a FEI Tecnai F20 microscope operating at 200 kV. The tomographic tilt series was acquired at 1° tilt increments to a maximum tile angular range of ±70° using the *Digital MicrographTM* (Gatan) STEM tomography module. Automated tomographic reconstruction was carried out using the DigiECT software package.

This instrument is also equipped with an Automatic Crystal Orientation Mapping (ACOM) system, which enables crystal orientation determination within intact WYHR-1 cells. This tool named "ASTAR" includes a precession device "DigiSTAR" and a dedicated scan generator. The ACOM measurements and data analyses were carried out according to the protocol described by Rauch et al. (2008). Briefly, precession electron diffraction (PED) spot patterns of magnetite particles were collected with a dedicated external CCD camera (8-bit color, 250 × 250 pixels picture size), while the sample area of interest was scanned by the electron beam. Scanning was performed with a beam spot size of 1.5 nm at a step size of 2 nm. Each frame has an exposure time of 25 ms (40 fps). Local crystallographic orientation(s) were obtained by comparing individually all spots in PED patterns via cross-correlation techniques with pre-calculated PED templates of magnetite (simulated for all possible crystal orientations); correct orientations were then determined by comparing/selecting templates with experimental PED patterns with the highest correlation index (Rauch et al., 2008). A correlation index map was assigned to the best match of each experimental pattern with the template. The reliability index was defined so that it had a minimum value when more than one solution was proposed and a high value when only one solution was identified clearly.

2.4. Cs-Corrected HAADF-STEM Imaging

Atomic resolution HAADF-STEM imaging and STEM-EDX (energy dispersive X-ray spectroscopy) analysis on both whole intact cells and individual magnetite particles from WYHR-1 were performed on a JEOL JEM-ARM200F microscope operating at 200 kV. The instrument is equipped with a double aberration-corrector for both probe-forming and imaging lenses and two silicon drift detectors with each detection area of 100 mm^2, which enables both atom-by-atom imaging and chemical mapping of materials (Kohno et al., 2010).

3. Results

3.1. Crystal Growth of WYHR-1 Magnetite Particles

Crystal growth was investigated by HRTEM observations on 93 magnetite particles with grain lengths ranging from ~8 to ~280 nm. Observed grain sizes are interpreted to reflect crystal growth stages because the smallest and largest grains are consistent with nascent and mature particles, respectively (Baumgartner et al., 2016; Li et al., 2009, 2015). Crystal length is plotted versus width in Figure 2 from HRTEM images

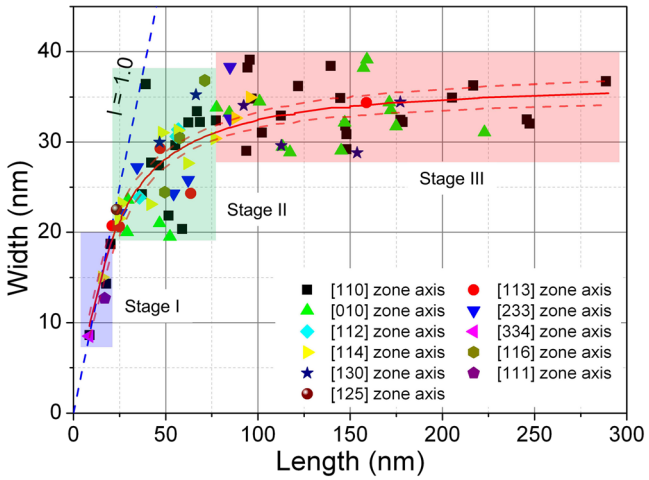

Figure 2. Plot of WYHR-1 magnetosomal crystal length versus width. Measurements were made on HRTEM images for individual magnetite particles each recorded from a given zone axis. Symbols with different colors indicate different zone axes. In total, 93 particles were analyzed in this study. Three-stage crystal growth is indicated. The red curve is a fit of the sigmoid function $W = a \tan^{-1}(bL)$, where $a = 23.57 \pm 1.03$, $b = 0.05 \pm 0.009$, and W and L are magnetite crystal width and length, respectively. Red dashed curves indicate the 95% confidence level about the fit.

of crystals imaged along various zone axes. Magnetosomal crystal growth in WYHR-1 occurs in a three-stage process. In Stage I, particles grow isotropically to ~20 nm with width/length ratio close to 1.0. In Stage II, they grow anisotropically to ~75 nm lengths and ~30–40 nm widths, with crystal length increasing faster than width. In Stage III, particles do not grow significantly in width and mainly grow in length to ~180 nm, with a few particles growing to ~280 nm (Figure 2).

Representative HRTEM images of particles smaller than ~30 nm are shown in Figure 3 (see Figure S2 for more TEM images and their corresponding analyses). Despite their perfect lattice and atomic structures, WYHR-1 magnetosomal crystal habits are difficult to determine for these small particles because clear crystal faces could not be identified. Small particles less than ~20 nm are nearly round (in 2-D projection) independent of the recording zone axis (Figures 3a–3c). In contrast, slightly larger particles (~20–30 nm) have irregular morphologies, which suggests that they have started anisotropic growth (Figures 3d–3f). Atomic structure imaging reveals that small magnetosomal crystal edges are ill-defined and appear to be amorphous or weakly crystalline (Figures 4 and S2). As shown in Figure 4 for a typical particle with ~8 nm size, the atomic arrangement of Fe ions and chemical composition of both Fe and O (Figures 4b–4f) indicates that it is magnetite. Meanwhile, two small weakly crystalline particles appear to be merging with this particle (Figure 4e). In agreement with a previous report from *Desulfovibrio magneticus* RS-1 (Baumgartner et al., 2016), this observation indicates that biomineralization of magnetite within strain WYHR-1 is preceded by a solid-state transformation of an iron precursor that could be required to produce asymmetric, elongated magnetite nanocrystals.

As particles reach threshold sizes of ~20 and ~75 nm, WYHR-1 magnetite particles start anisotropic and unidirectional growth, respectively. As shown in Figure 5, TEM observations on crystals with different sizes and

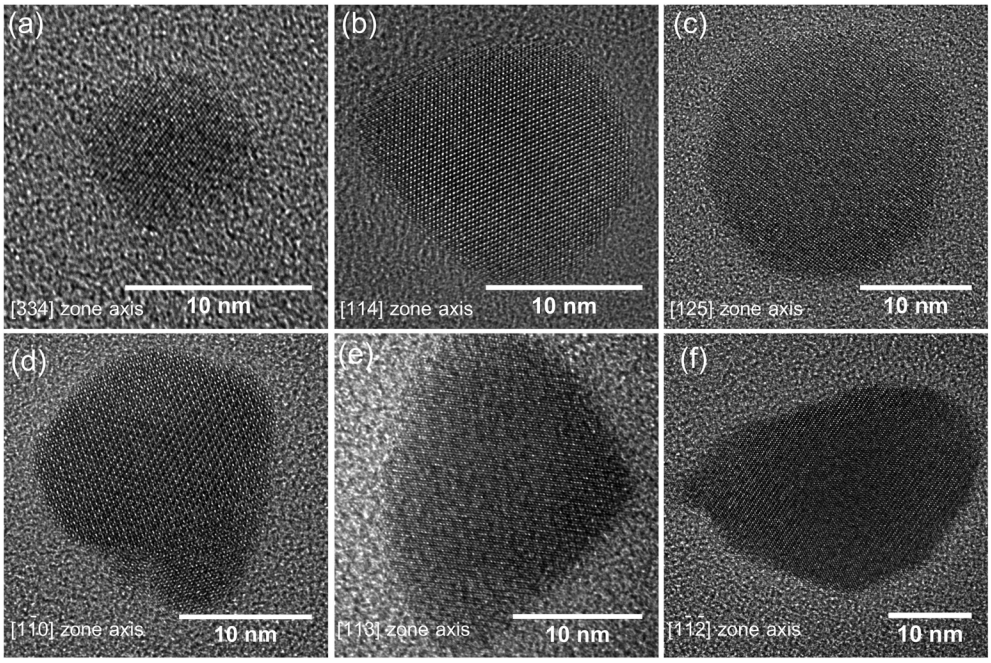

Figure 3. HRTEM images of WYHR-1 magnetosomal magnetite with crystals smaller than ~30 nm. Small particles generally have nearly round 2-D projected shapes (a–c), whereas slightly larger particles are elongated and asymmetric (d–f).

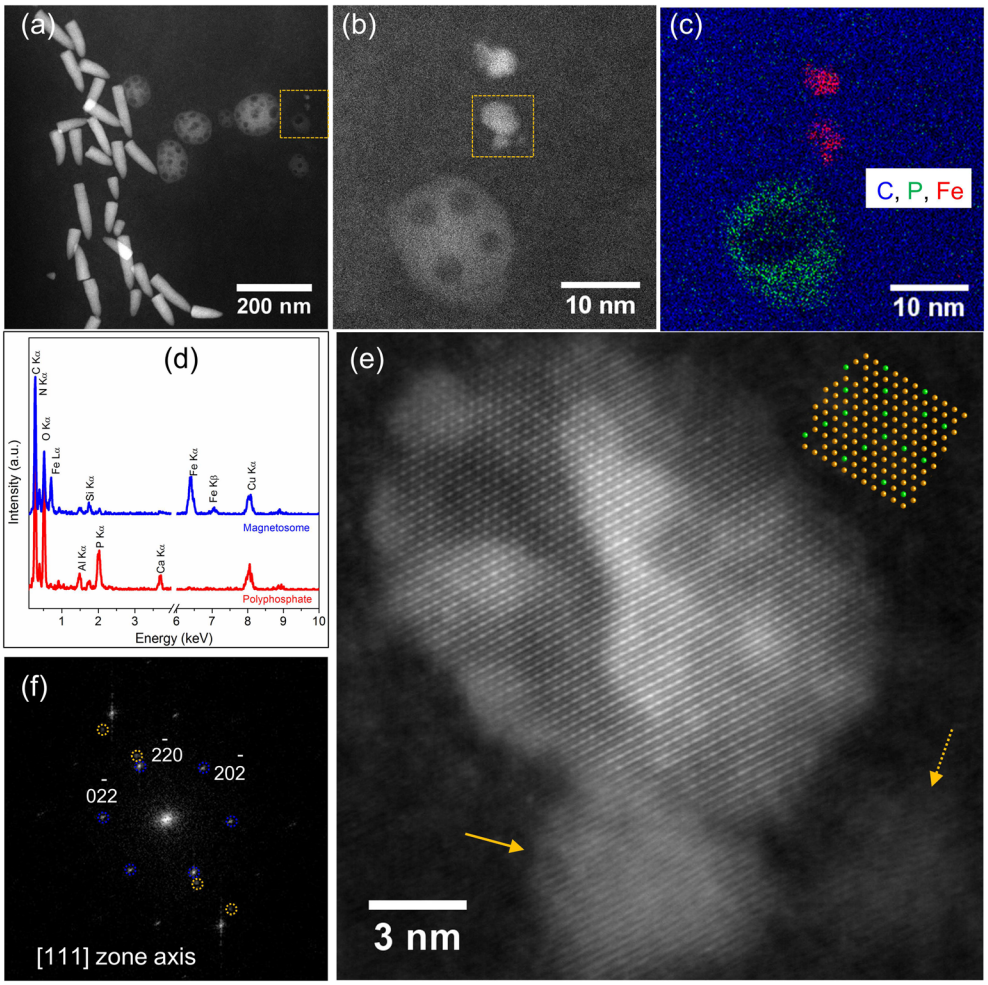

Figure 4. Morphological, chemical, and structural features of a WYHR-1 magnetosomal magnetite with ~8 nm size analyzed by atomic-resolution HAADF-STEM. (a) HAADF-STEM image of a region of the WYHR-1 cell. Two small magnetite particles and one polyphosphate inclusion occur within the yellow dashed box. Holes in the polyphosphate inclusions result from EDX beam damage. (b) Close-up of the area outlined by the yellow dashed box in Figure 4a. (c) Chemical composition map of the same area in Figure 4b. The C-, P-, and Fe-Kα distributions are indicated in blue, green, and red, respectively. (d) EDX spectra of the polyphosphate inclusion (red) and magnetite particle (blue) as shown in Figure 4b. (e) Atomic structure of the magnetite particle indicated by the yellow dashed box in Figure 4b. The theoretical Fe arrangement of magnetite is shown in the inset for comparison; yellow and green balls indicate octahedral and tetrahedral Fe, respectively. Two small weakly or non-crystalline particles are close to (yellow dashed arrow) and merging with (yellow arrow) the particle. (f) Corresponding fast Fourier transform (FFT) index for the upper particle and the lower left particle in Figure 4e. White dots marked by blue dashed circles are the FFT diffraction pattern (reciprocal space) of the upper particle in Figure 4e, and relatively weak white dots marked by yellow dashed circles are from the lower left particle in Figure 4e.

from different zone axes consistently reveal that WYHR-1 magnetite elongates exclusively along the [001] direction of magnetite. The elongation direction is also parallel to the crystal long axis in both anisotropic and unidirectional growth stages (Figures 5, S3, S4, and S5). With growth, the crystal changes its morphology gradually from a teardrop to a bullet shape. Specifically, immature particles have teardrop morphologies without obvious crystal faces (Figures 5a, 5d, and 5g). With increasing width and length during the anisotropic growth stage, the crystal bases (i.e., the wider end of particles) become flatter, resulting in nearly triangular shapes (Figures 5b, 5e, and 5h). During final stages of unidirectional growth, crystals elongate continuously along the [001] direction, while crystal width remains roughly constant (~30–40 nm) (Figures 5c, 5f, and 5i).

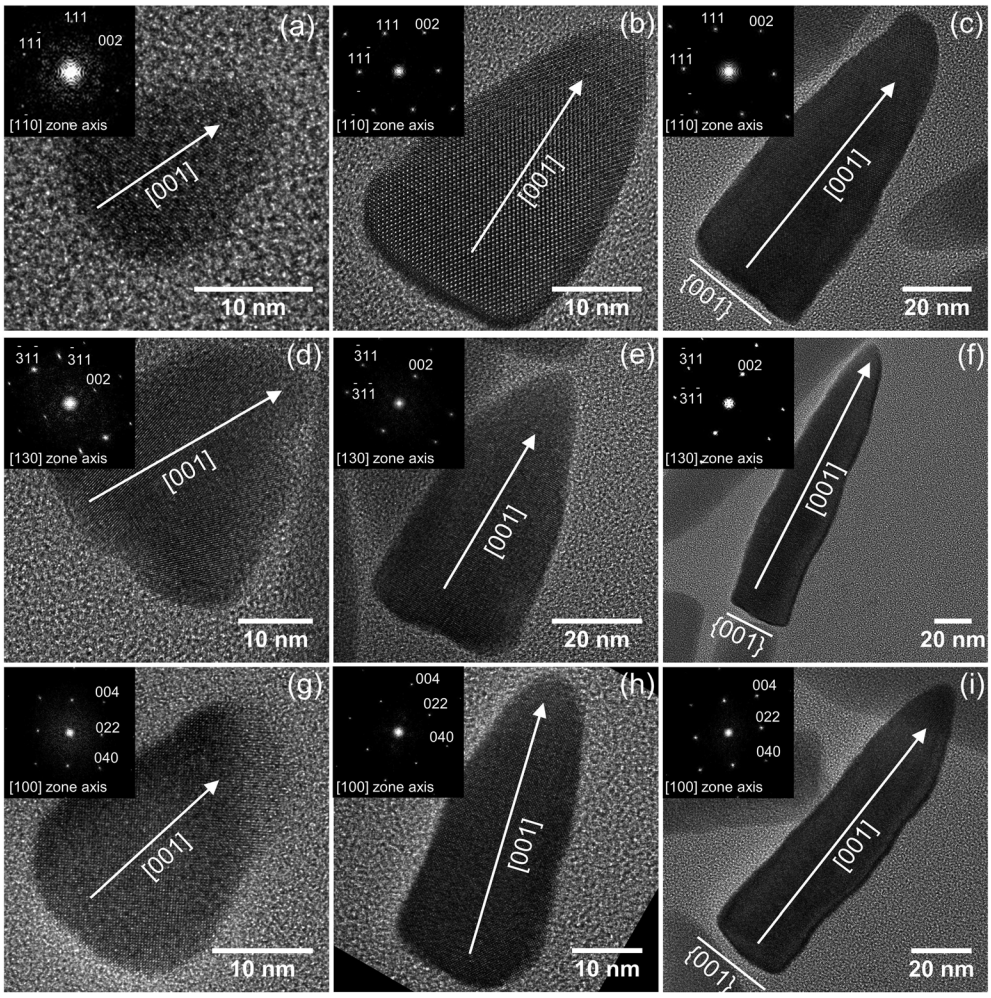

Figure 5. HRTEM images of particles with crystal size larger than ~20 nm that illustrate anisotropic and unidirectional crystal growth of WYHR-1 magnetite particles. Corresponding indexed FFT patterns for each particle are shown as insets in the upper left corner of each panel. TEM images of (a–c) [1$\bar{1}$0] zone axis of magnetite, (d–f) [130] zone axis, and (g–i) [100] zone axis. From left to right, the first column represents immature particles with teardrop morphologies, the second represents larger immature particles with triangular morphologies, and the third represents mature particles with bullet-shaped morphologies. HRTEM observations of various particles with different sizes from different zone axes consistently reveal that the [001] crystal direction of magnetite is parallel to its elongation direction as indicated by white arrows.

3.2. Crystal Morphology and Ideal Habit of WYHR-1 Magnetosomes

Both HRTEM and atomic-resolution HAADF-STEM observations reveal that WYHR-1 magnetosomes contain single magnetite crystals without obvious defects (Figures 3–6 and S2–S5). For mature elongated crystals, the basal end is terminated by one large {001} face, while the tip is conical (Figure 6). The crystal edges do not have obvious faces for either immature or mature elongated particles (Figures 5, 6, and S3–S5). HAADF-STEM tomography on individual particles reveals clearly the 3-D morphology of WYHR-1 magnetosomes, which are long bullet-shaped cylinders with a flat base and conical tip (Figure 6e and Movie S1). These observations, therefore, enable development of an ideal morphological model for WYHR-1 magnetite (Figure 6f). It has a long cylinder with one large {001} bottom surface and many high-index edge faces (blue regions) that form the base, with an elongated cone and mostly high-index edge faces (green, yellow, and aqua regions) at the top. The elongation axis of WYHR-1 magnetosomal magnetite is parallel to the [001] crystal direction of magnetite.

Notably, this model does not represent the kinked magnetite particles observed occasionally within WYHR-1. HRTEM observations on kinked particles reveal variable initial elongation directions including

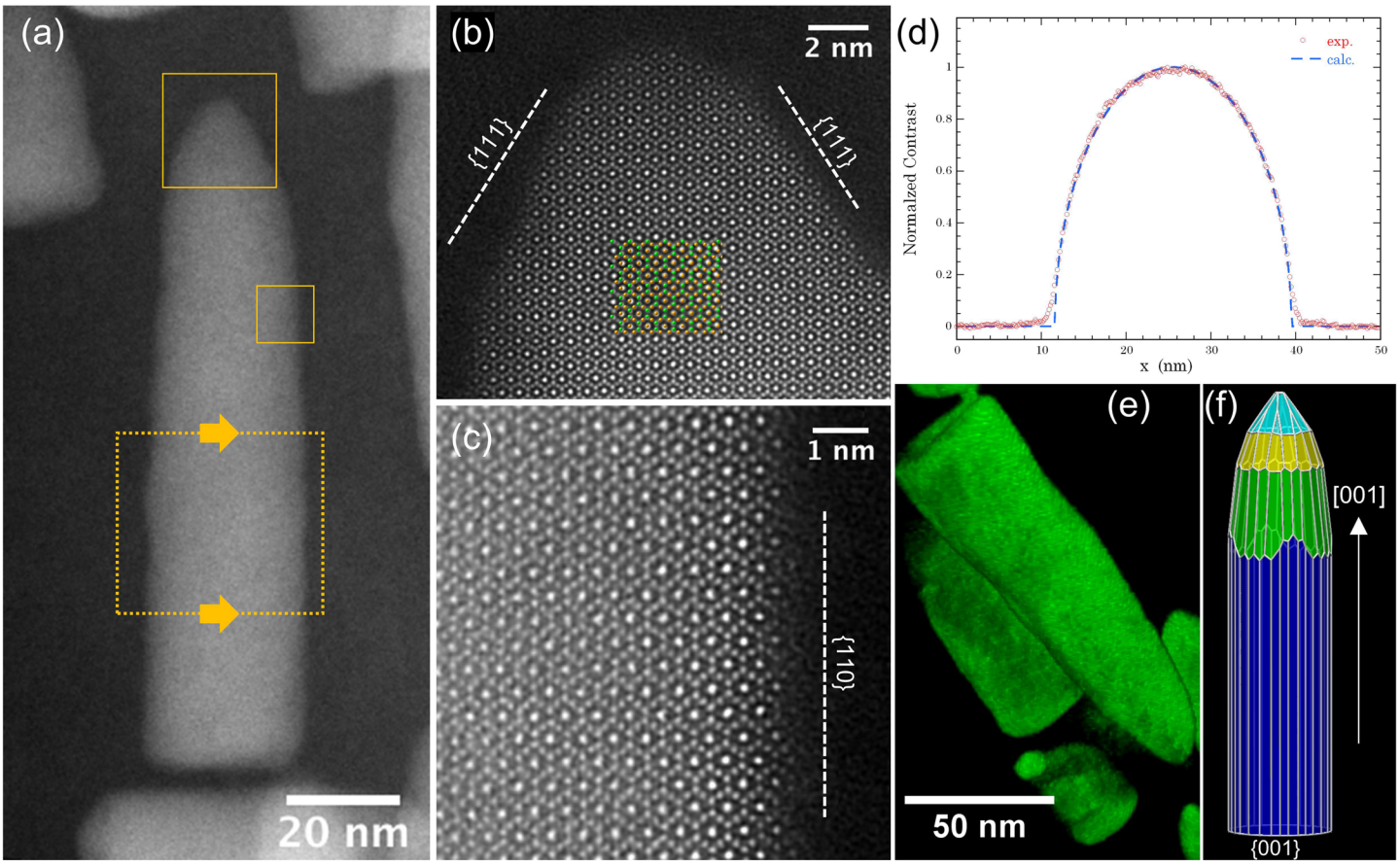

Figure 6. Atomic structure and 3-D morphology of WYHR-1 magnetosomal crystals. (a) HAADF-STEM image of a mature WYHR-1 magnetosomal crystal from the [1$\bar{1}$0] zone axis. (b, c) Atomic structure of the top and side of the particle shown in Figure 6a indicated by the solid yellow boxes. The theoretical Fe arrangement for magnetite is shown in Figure 6b as an overlap inset for comparison; yellow and green balls indicate octahedral and tetrahedral Fe, respectively. (d) Normalized contrast profile across the yellow dashed box in the HAADF-STEM image in Figure 6a. The intensity profile is proportional to particle thickness. Therefore, the image contrast profile from the experimental HAADF-STEM image is comparable to that calculated for a cylinder, which provides evidence that WYHR-1 magnetite particles have round sides like a cone rather than a prism. (e) Tomographic reconstruction image (3-D visualization) of WYHR-1 magnetite particles. (f) Morphological model for WYHR-1 magnetosomal magnetite. It is a long cylinder terminated by a {001} face at the bottom end and an elongated cone at the top end. Blue regions are crystal faces that form the side of the cylinder, and green, yellow, and aqua regions indicate crystal faces that form the sides of the elongated cone.

[011] and [111]. However, the final elongation direction is uniform along [001], despite different initial elongation directions (Figure S6).

3.3. Chain Assembly and Crystal Orientation of WYHR-1 Magnetosomal Magnetite

The chain structure of WYHR-1 magnetosomal crystals was investigated by combining HAADF-STEM tomography and ACOM (Figure 7). Experimental results demonstrate that bullet-shaped particles within WYHR-1 are organized into a single straight bundle that extends along the cell long axis following the cell curvature. Every bundle generally consists of two to three closely packed and approximately parallel chains, so that individual particle long axes are approximately parallel to the chain direction (Figure 7b and Movie S2). Particle tips do not all point in the same direction; ~80% of particles are aligned in the same direction, with others in the opposite direction.

ACOM orientation mapping indicates that almost all particles within chains are oriented close to the [001] direction of magnetite, consistent with HRTEM observations on individual particles (Figures 7c–7i). As expected, all WYHR-1 crystals resemble magnetite, as indicated by the correlation index map in which crystals appear as white to light gray pixels (Figures 7c and 7d). These indications are consistent everywhere in the chains, except for a few particles (with black to light gray pixels) likely due to grain thickness variations or to overlapping particles (Figure 7e). The *x*, *y*, and *z* orientation maps (multiplied by index map) indicate

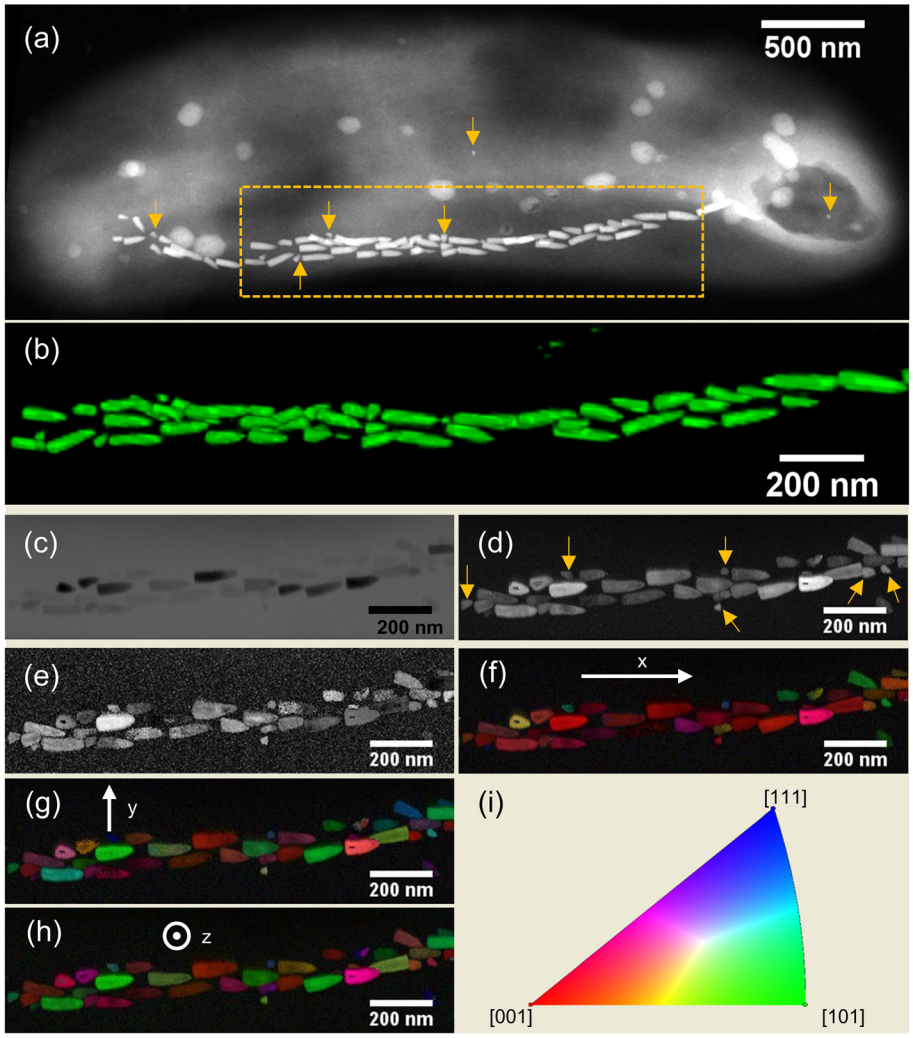

Figure 7. Chain assembly (a, b) and crystal orientation (c–i) of bullet-shaped particles within WYHR-1. (a) HAADF-STEM image of a WYHR-1 cell that was selected for HAADF-STEM tomography analysis. (b) HAADF-STEM tomographic reconstruction image (3-D visualization) of magnetosomal magnetite indicated by the yellow dashed rectangle in Figure 7a. (c–i) ACOM orientation mapping of WYHR-1 chains. (c) Virtual bright field map, (d) correlation index map, (e) reliability index map, (f) *x* orientation map, (g) *y* orientation map, (h) *z* orientation map, and (i) color key. The small particles inside and away from the chains are indicated by the yellow arrows in Figures 7a and 7d. Precession angle, beam spot size: 1.5 nm, scanning step size: 2 nm, condenser aperture: 50 μm, camera length: 89 mm.

clearly that WYHR-1 crystals are well ordered only along the chain direction, which indicates that, except for several small or misaligned particles, all particles have the same crystal orientation (along *x*), that is, with [001] zone axes chain-parallel (Figure 7f). However, chain-perpendicular [110] crystal axes have two distinct directions (*y* and *z* orientations), that is, they do not correlate with each other (Figures 7g and 7h). Consistent with observations of prismatic particles with [111]-crystal elongation and chain orientation (Pósfai, Kasama, & Dunin-Borkowski, 2013), this result confirms a chain structure of beads on a string, in which individual crystals have a fixed direction along chains and rotate freely about the chain.

4. Discussion

4.1. Chain Assembly and Crystal Growth Pattern of WYHR-1 Magnetosomal Magnetite

The crystal growth and orientation of bullet-shaped particles within magnetotactic Deltaproteobacteria have not been studied in detail, although morphological and crystallographic features have been reported for MTB strains RS-1 (Baumgartner et al., 2016; Pósfai et al., 2006), AV-1 (Lefèvre, Pósfai, et al., 2011), BW-1

(Descamps et al., 2017), and *Candidatus* Magnetananas tsingtaoensis (Zhou et al., 2012). We here present a comprehensive microscopic study of WYHR-1 magnetosomal magnetite at both chain and particle levels, in both 2-D and 3-D at nanometer and atomic resolution. Our results indicate that WYHR-1 organizes crystals into a single straight bundle of multiple chains (generally two to three chains) that are closely packed and nearly parallel to one another along the cell long axis following the cell curvature (Figures 7a and 7b). They assemble along the [001] crystal direction of magnetite, that is, they have a uniform crystal orientation along the chain direction (Figures 7c–7i). As a result, the chain direction is parallel to the elongation directions of individual particles. Such a chain configuration along with highly elongated morphologies of individual particles ensures that the effective magnetic dipole moment of the entire chain is suitable for magnetotaxis. This is because the strong shape anisotropy of individual particles along their [001] magnetocrystalline hard axis and intrachain magnetic interactions combine to overcome completely the negative effect of magnetocrystalline anisotropy (Chariaou et al., 2015; Körnig et al., 2014; Li et al., 2010, 2015).

Crystal habit and magnetite growth in WYHR-1 appear to be species-specific. First, beside other physical features such as grain size and chain structure, the crystal habit differs from that of magnetosomal magnetite in other Deltaproteobacteria MTB (Pósfai, Lefèvre, et al., 2013). For instance, magnetite in MTB strain AV-1 has a double-triangle shape in 2-D projections, which can be modeled as a slightly elongated, half-octahedron (four-sided pyramid) at the basal end and an elongated point with mostly high-index faces (Lefèvre, Pósfai, et al., 2011). In contrast, magnetosomal magnetite in WYHR-1 is highly elongated and bullet-shaped, which can be modeled as a long cylinder with one large {001} bottom surface and many high-index edge faces on the cylinder and an elongated cone consisting mostly of high-index edge faces at the tip (Figure 6).

Second, the crystal habit and growth pattern both differ from that of bullet-shaped particles produced by MTB of the Nitrospirae phylum. Within *Candidatus* Magnetobacterium casensis strain MYR-1, for instance, particles grow isotropically to ~40 nm to form initial cubo-octahedral crystals, followed by anisotropic growth to ~60–80 nm with elongation mostly along the [112], [113], [114], [115], or even [111] directions of magnetite, and finally kink and grow continuously along the [001] direction to ~200 nm (Li et al., 2015). Mature MYR-1 particles are highly elongated and kinked and are terminated by a large {111} face at the larger basal end and a small {001} face at the top (Li et al., 2015). For *Candidatus* Thermomagnetovibrio paiutensis strain HSMV-1, many bullet-shaped particles are also bent, highly elongated along the [110] direction and terminated by one large {110} face at the larger basal end (Lefèvre, Pósfai, et al., 2011). By comparison, WYHR-1 particles grow isotropically to ~20 nm, to form nearly round particles without obvious crystal faces. Subsequently, they grow anisotropically along the magnetite [001] direction to ~75 nm in length and ~30–40 nm in width. In the final stage, they grow continuously in length along the [001] direction to ~180 nm, with a few up to ~280 nm, but with the crystal width remaining roughly constant. Mature WYHR-1 particles are straight and bullet-shaped with a large {001} face at the basal end and a conical tip (Figure 6).

Third, crystal growth and morphology in strains WYHR-1 (this study), AV-1 (Lefèvre, Pósfai, et al., 2011), and MYR-1 (Li et al., 2015) differ significantly from those in MTB of the Alphaproteobacteria and Gammaproteobacteria classes. Magnetotactic Alphaproteobacteria and Gammaproteobacteria generally biomineralize magnetite with symmetric morphologies, including octahedra ({111} forms) (Araujo et al., 2016; Zhang et al., 2017), cubo-octahedra ({111} + {100} forms) (Faivre et al., 2008; Li, Ge, et al., 2013; Mann et al., 1984), and elongated hexagonal prisms ({111} + {110} + {100} forms) (Li et al., 2017; Meldrum et al., 1993a, 1993b). Unlike the multiple-step growth for elongated asymmetric crystals observed in strains WYHR-1 (this study), AV-1 (Lefèvre, Pósfai, et al., 2011), and MYR-1 (Li et al., 2015), symmetric crystals generally have homothetical growth, that is, constant width/length ratio in a given MTB species (Lefèvre, Trubitsyn, Abreu, Kolinko, Jogler, & de Almeida, 2013; Li et al., 2017; Meldrum et al., 1993a, 1993b; Sparks et al., 1990; Zhang et al., 2017). In addition, small (immature) magnetite particles are usually distributed randomly within chains and even away from chains within WYHR-1 cells (Figures 1 and 7). These particles are different from the symmetric crystals that are generally located at the ends of chain(s) (Li et al., 2017; Li, Ge, et al., 2013; Mann et al., 1984; Meldrum et al., 1993a, 1993b; Sparks et al., 1990; Zhang et al., 2017), indicating a different mechanism of magnetosome chain assembly between symmetric and asymmetric particles.

Finally, a few studies have shown that magnetotactic eukaryotic single-celled organisms (e.g., algae and protists) can also biomineralize magnetite (Leão et al., 2020; Torres de Araujo et al., 1986). By combining TEM

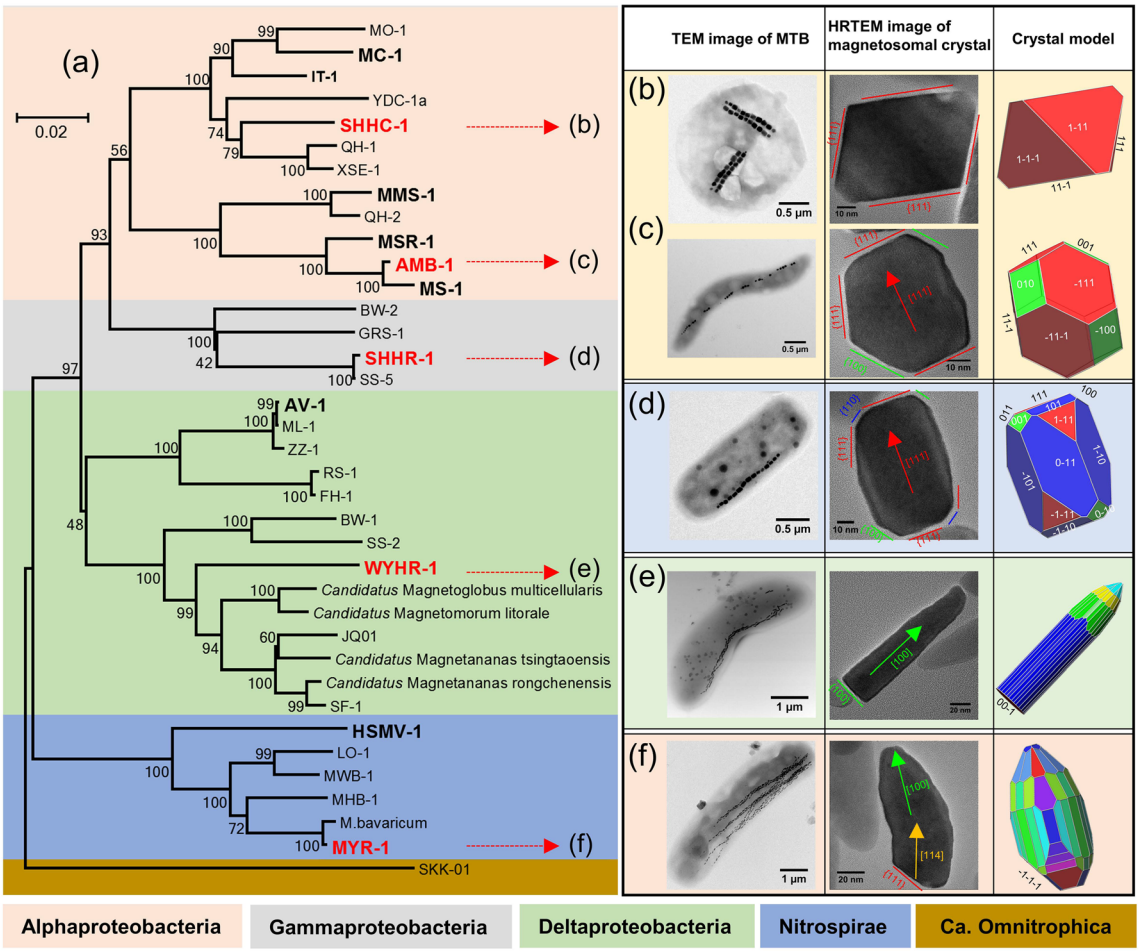

Figure 8. Relationship between bacterial phylogeny and magnetosomal magnetite morphology. (a) Phylogenetic tree based on 16S rRNA gene sequences. Bootstrap values (>50) at nodes are percentages of 1,000 replicates. The 16S rRNA gene sequence of the MTB *Candidatus* Omnitrophus magneticus SKK-01 was used to root the tree. Particle morphology for (b) magnetotactic Alphaproteobacteria strain SHHC-1 (Zhang et al., 2017), (c) magnetotactic Alphaproteobacteria strain AMB-1 (Li, Ge, et al., 2013), (d) magnetotactic Gammaproteobacteria strain SHHR-1 (Li et al., 2017), (e) magnetotactic Deltaproteobacteria strain WYHR-1 (this study), and (f) magnetotactic Nitrospirae strain MYR-1 (Li et al., 2015). From panel (b) to panel (f), the first column contains TEM images of MTB cells, the second contains HRTEM images of individual crystals recorded from [1$\bar{1}$0] zone axis of magnetite, and the third contains the corresponding crystal models.

and synchrotron-based scanning transmission X-ray microscopy (STXM), Leão et al. (2020) found that a novel magnetotactic flagellated protozoan produces anisotropic, bullet-shaped, magnetite that is also elongated along the [001] direction and is organized into straight multiple chain bundles. However, crystal length versus width and shape factor distributions for the bullet-shaped crystals produced by the protist are significantly different from those for MTB. They have a mean length of 276.6 ± 61.3 nm and a mean shape factor of 0.2 ± 0.04 (Leão et al., 2020) and are, therefore, much longer and more elongated than the bullet-shaped crystals produced by all MTB known so far (Descamps et al., 2017; Lefèvre, Pósfai, et al., 2011; Li et al., 2015, 2019; Pósfai et al., 2006; Pósfai, Lefèvre, et al., 2013; Zhou et al., 2012).

4.2. Implications for Magnetosomal Biomineralization and Magnetofossil Identification

Taking the phylogenetic positions of MTB into account, a relationship between bacterial phylogeny and magnetosomal magnetite morphology can be found (Figure 8). First, MTB within the deep-branching bacterial phylum Nitrospirae or class Deltaproteobacteria tend to produce more asymmetric (either kinked or straight bullet-shaped) magnetosomal magnetite with fewer crystal faces. In contrast, young-branching bacterial classes such as magnetotactic Alphaproteobacteria and Gammaproteobacteria prefer to synthesize symmetric (prismatic, cubo-octahedral, or octahedral) magnetite particles with more crystal faces. Second, bullet-shaped magnetite particles are generally elongated and assembled along the magnetocrystalline

hard axis [001] (e.g., WYHR-1 and MYR-1) (Li et al., 2015; this study) or intermediate magnetization direction [110] (e.g., HSMV-1) (Lefèvre, Pósfai, et al., 2011), which results in a lower maximum magnetic moment along the chain direction (Kirschvink, 1992). This might explain partially why MTB belonging to the Nitrospirae phylum and the Deltaproteobacteria class generally biomineralize a large number of magnetite crystals to produce a magnetic moment strong enough for magnetotaxis. Due to natural selection maximizing the efficiency with which MTB employ Fe, magnetotactic Alphaproteobacteria and Gammaproteobacteria produce prismatic and cubo-octahedral magnetite that are always elongated and assembled along the magnetocrystalline easy axis [111] (Kopp & Kirschvink, 2008). This crystal habit and chain assembly maximize the magnetic moment along the chain direction due to a joint effect of positive magnetocrystalline anisotropy, shape anisotropy, and intrachain interactions (Dunin-Borkowski et al., 1998; Li, Ge, et al., 2013). Third, as discussed above, the crystal growth and habit of magnetite crystals are also related closely to taxonomic group and even species in MTB. It appears that the crystal growth and habit for different taxonomic lineages are more different than those within closely related groups. This indicates strongly that magnetite biomineralization is likely to be group-specific or even species-specific.

It has been demonstrated that magnetosomal biomineralization is controlled strictly by a group of conserved MGCs that vary in gene content and organization among different MTB taxonomic groups and species (Grünberg et al., 2001; Lefèvre & Bazylinski, 2013; Lin, Deng, et al., 2014; Lin et al., 2018; Murat et al., 2010). Several *mam* (magnetosome membrane) genes (*mamABEKMOPQI*) have been identified in all MTB genomes studied to date (*mamL* is additionally present in all MTB that produce only magnetite) (Ji et al., 2017; Lefèvre, Trubitsyn, Abreu, Kolinko, Jogler, & de Almeida, 2013; Lin, Deng, et al., 2014). This suggests that these core genes control universal processes in all MTB, such as the biogenesis and assembly of the magnetosome membrane, Fe^{2+} uptake, magnetite biomineralization, and chain assembly (Komeili, 2012; Toro-Nahuelpan et al., 2019; Uebe & Schüler, 2016). MGC variability accounts for diverse crystal composition, shape, size, number, and intracellular organization of crystals and possibly results in species-specific magnetite biomineralization in MTB. For instance, homologs of the *mamGFDC* and *mms* (magnetic particle-membrane specific) operons are only found in the magnetotactic Alphaproteobacteria, which suggests that these genes control biomineralization of octahedral, cubo-octahedral, and elongated prismatic magnetite crystals (Ji et al., 2017). On the other hand, various families of *mad* (magnetosome-associated Deltaproteobacteria) genes that are specifically present in the genomes of magnetotactic Deltaproteobacteria suggest that they are associated with highly elongated and bullet-shaped magnetite crystals (Lefèvre Trubitsyn, Abreu, Kolinko, Jogler, & de Almeida, 2013). Both mad and man (a magnetosome gene specific to Nitrospirae) coexist in MTB from the Nitrospirae and Omnitrophica phyla, which suggests that the joint function of *mad* and *man* genes contributes to biomineralization of highly elongated, kinked, and bullet-shaped magnetite crystals (Lin et al., 2018; Lin, Deng, et al., 2014). In summary, MGC gene content and organization vary among MTB taxonomic groups and species and are related closely to crystal growth and habits. Considering that gene content and organization in each MGC correspond to MTB bacterial taxonomies (Lefèvre, Trubitsyn, Abreu, Kolinko, de Almeida, & de Vasconcelos, 2013; Lefèvre, Trubitsyn, Abreu, Kolinko, Jogler, & de Almeida, 2013; Lin et al., 2017, 2018), crystal growth and habits can, therefore, be related closely to MTB taxonomic group or species. This indicates that magnetofossils might not only be ideal paleomagnetic remanence carriers but that their crystal growth pattern and crystallographic features could also be used to indicate ancient MTB taxonomy. Acquisition of such phylogenetic and biological information from magnetofossils could provide direct clues about the evolution of biomineralization and magnetotaxis within MTB and the interplay between MTB and ancient environments.

It should be noted that the physical (e.g., morphology and crystal size distribution), chemical (e.g., stoichiometry and cation-substitution), and even crystallographic features of magnetosomal magnetite could be modified to some extent by the environments in which MTB live (Faivre et al., 2008; Lefèvre et al., 2016; Li et al., 2016; Li & Pan, 2012; Olszewska-Widdrat et al., 2019). Microscopic identifications of magnetofossils tend to rely on morphological recognition based on conventional TEM observations (Chang et al., 2018; Li, Benzerara, et al., 2013; Yamazaki et al., 2019), which fail to acquire detailed information on crystal growth and habit and sometimes result in magnetofossil misidentification (Buseck et al., 2001). Therefore, additional systematic studies of magnetosomal crystals in both modern MTB and magnetotactic eukaryotes, and magnetofossils from ancient sediments with various combined advanced TEM and STXM approaches are vital (Buseck et al., 2001; Kalirai et al., 2013; Leão et al., 2020; Li, Benzerara, et al., 2013; Zhu

et al., 2016). In addition, studies of magnetosomal biomineralization in MTB grown in controlled laboratory conditions are still needed to expand our knowledge of the relationship between crystal growth and MTB phylogeny and/or environmental factors (Faivre et al., 2008; Lefèvre et al., 2016; Li et al., 2009; Li & Pan, 2012).

5. Conclusions

We carried out a systematic investigation of magnetosomal crystal growth and chain arrangements within a novel magnetotactic Deltaproteobacteria strain WYHR-1 using advanced TEM techniques from micron to atomic scales. WYHR-1 magnetosomal crystals grow in a multistep pattern that can be divided into three stages: (i) initial isotropic growth up to ~20 nm forming nearly round magnetite particles, (ii) subsequent anisotropic growth along the [001] crystal direction of magnetite up to ~75 nm in length and ~30–40 nm in width, and (iii) unidirectional growth continuously along the [001] direction to ~180 nm length, with some growing as large as ~280 nm. Most mature WYHR-1 magnetite crystals have a characteristic bullet-shaped with one large {001} face at the base and a conical tip.

Within each WYHR-1 cell, all particles are organized into one straight bundle generally consisting of two to three chains packed close and nearly parallel to each other. Almost all particles within chains are assembled along the [001] crystal direction of magnetite, that is, they have uniform crystal orientation along the chain direction. Parallelism between the chain direction and elongation direction of individual particles ensures effective magnetic dipole confinement along the chain direction that assists magnetotaxis.

The crystal habit and growth pattern of WYHR-1 magnetite is different from those of bullet-shaped magnetite crystals produced by other MTB from the Deltaproteobacteria and Nitrospirae, which indicates species-specific magnetite biomineralization in MTB. This suggests that the crystal habit of magnetofossils from the geological record might enable development of a proxy for taxonomic groups or species of ancient MTB and interpretation of environments in which ancient MTB lived.

Data Availability Statement

All images reported in this manuscript are available in Figures S1–S6 and Movie S1–S2 in the supporting information. All of the data used to build Figure 2 of this paper are available in Figshare (https://doi.org/10.6084/m9.figshare.11743272).

Acknowledgments

The authors thank Professors Richard Frankel and Shucheng Xie for constructive comments that improved the original manuscript. J. H. L. benefited from discussions in Office 442 of the IGGCAS. This study was supported financially by the National Natural Science Foundation of China (grants no. 41920104009, 41890843, and 41621004), The Senior User Project of RVKEXUE2019GZ06 (Center for Ocean Me Mega-Science, Chinese Academy of Sciences), and the Australian Research Council (grant DP160100805). HRTEM experiments were performed on a JEOL JEM-2100F microscope installed at the Institut de minéralogie, de physique des matériaux et de cosmochimie (IMPMC) - Sorbonne Université and CNRS (Paris, France). HAADF-STEM tomography and ACOM experiments were carried out on a FEI Tecnai F20 microscope installed at the Institut de Chimie et des Matériaux de Paris Est (ICMPE) – CNRS (Thiais, France). Atomic resolution HAADF-STEM and STEM-EDX mapping experiments were done on a JEOL JEM-ARM200F microscope installed at the Institute of Physics, Chinese Academy of Sciences (IPCAS) (Beijing, China).

References

Abreu, F., Silva, K. T., Leão, P., Guedes, I. A., Keim, C. N., Farina, M., & Lins, U. (2013). Cell adhesion, multicellular morphology, and magnetosome distribution in the multicellular magnetotactic prokaryote Candidatus Magnetoglobus multicellularis. *Microscopy and Microanalysis*, *19*(3), 535–543. https://doi.org/10.1017/S1431927613000329

Amor, M., Busigny, V., Durand-Dubief, M., Tharaud, M., Ona-Nguema, G., & Gélabert, A. (2015). Chemical signature of magnetotactic bacteria. *Proceedings of the National Academy of Sciences, USA*, *112*(6), 1699–1703. https://doi.org/10.1073/pnas.1414112112

Araujo, A. C. V., Morillo, V., Cypriano, J., Teixeira, L. C. R. S., Leão, P., & Lyra, S. (2016). Combined genomic and structural analyses of a cultured magnetotactic bacterium reveals its niche adaptation to a dynamic environment. *BMC Genomics*, *17*(S8), 726–462. https://doi.org/10.1186/s12864-016-3064-9

Baumgartner, J., Menguy, N., Gonzalez, T. P., Morin, G., Widdrat, M., & Faivre, D. (2016). Elongated magnetite nanoparticle formation from a solid ferrous precursor in a magnetotactic bacterium. *Journal of the Royal Society Interface*, *13*, 20160665. https://doi.org/10.1098/rsif.2016.0665

Bazylinski, D. A., & Frankel, R. B. (2004). Magnetosome formation in prokaryotes. *Nature Reviews Microbiology*, *2*(3), 217–230. https://doi.org/10.1038/nrmicro842

Buseck, P. R., Dunin-Borkowski, R. E., Devouard, B., Frankel, R. B., McCartney, M. R., & Midgley, P. A. (2001). Magnetite morphology and life on Mars. *Proceedings of the National Academy of Sciences, USA*, *98*(24), 13,490–13,495. https://doi.org/10.1073/pnas.241387898

Chang, L., Harrison, R. J., Zeng, F., Berndt, T. A., Roberts, A. P., & Heslop, D. (2018). Coupled microbial bloom and oxygenation decline recorded by magnetofossils during the Palaeocene–Eocene thermal maximum. *Nature Communications*, *9*, 4007. https://doi.org/10.1038/s41467-018-06472-y

Chariaou, M., Rahn-Lee, L., Kind, J., García-Rubio, I., Komeili, A., & Gehring, A. U. (2015). Anisotropy of bullet-shaped magnetite nanoparticles in the magnetotactic bacteria *Desulfovibrio magneticus* sp. strain RS-1. *Biophysical Journal*, *108*(5), 1268–1274. https://doi.org/10.1016/j.bpj.2015.01.007

Chen, Y. R., Zhang, R., Du, H. J., Pan, H. M., Zhang, W. Y., & Zhou, K. (2015). A novel species of ellipsoidal multicellular magnetotactic prokaryotes from Lake Yuehu in China. *Environmental Microbiology*, *17*(3), 637–647. https://doi.org/10.1111/1462-2920.12480

Descamps, E. C. T., Monteil, C. L., Menguy, N., Ginet, N., Pignol, D., & Bazylinski, D. A. (2017). *Desulfamplus magnetovallimortis* gen. nov., sp nov., a magnetotactic bacterium from a brackish desert spring able to biomineralize greigite and magnetite, that represents a novel lineage in the *Desulfobacteraceae*. *Systematic and Applied Microbiology*, *40*(5), 280–289. https://doi.org/10.1016/j.syapm.2017.05.001

Dunin-Borkowski, R. E., McCartney, M. R., Frankel, R. B., Bazylinski, D. A., Pósfai, M., & Buseck, P. R. (1998). Magnetic microstructure of magnetotactic bacteria by electron holography. *Science*, *282*(5395), 1868–1870. https://doi.org/10.1126/science.282.5395.1868

Faivre, D., Menguy, N., Pósfai, M., & Schüler, D. (2008). Environmental parameters affect the physical properties of fast-growing magnetosomes. *American Mineralogist*, *93*(2–3), 463–469. https://doi.org/10.2138/am.2008.2678

Grünberg, K., Wawer, C., Tebo, B. M., & Schüler, D. (2001). A large gene cluster encoding several magnetosome proteins is conserved in different species of magnetotactic bacteria. *Applied and Environmental Microbiology*, *67*(10), 4573–4582. https://doi.org/10.1128/AEM.67.10.4573-4582.2001

Ji, B., Zhang, S. D., Zhang, W. J., Rouy, Z., Alberto, F., & Santini, C. L. (2017). The chimeric nature of the genomes of marine magnetotactic coccoid-ovoid bacteria defines a novel group of Proteobacteria. *Environmental Microbiology*, *19*(3), 1103–1119. https://doi.org/10.1111/1462-2920.13637

Jogler, C., Wanner, G., Kolinko, S., Niebler, M., Amann, R., & Petersen, N. (2011). Conservation of proteobacterial magnetosome genes and structures in an uncultivated member of the deep-branching Nitrospira phylum. *Proceedings of the National Academy of Sciences, USA*, *108*(3), 1134–1139. https://doi.org/10.1073/pnas.1012694108

Kalirai, S. S., Bazylinski, D. A., & Hitchcock, A. P. (2013). Anomalous magnetic orientations of magnetosome chains in a magnetotactic bacterium: *Magnetovibrio blakemorei* strain MV-1. *PLoS ONE*, *8*, e53368. https://doi.org/10.1371/journal.pone.0053368

Kirschvink, J. L. (1992). On the magnetostatic control of crystal orientation and iron accumulation in magnetosomes. *Automedica*, *14*, 257–269.

Kohno, Y., Okunishi, E., Tomita, T., Ishikawa, I., Kaneyama, T., & Ohkura, Y. (2010). Development of a cold field-emission gun for a 200kV atomic resolution electron microscope. *Microscopy and Analysis*, *24*(7), S9–S13.

Kolinko, S., Jogler, C., Katzmann, E., Wanner, G., Peplies, J., & Schüler, D. (2012). Single-cell analysis reveals a novel uncultivated magnetotactic bacterium within the candidate division OP3. *Environmental Microbiology*, *14*(7), 1709–1721. https://doi.org/10.1111/J.1462-2920.2011.02609.X

Kolinko, S., Richter, M., Glockner, F. O., Brachmann, A., & Schüler, D. (2014). Single-cell genomics reveals potential for magnetite and greigite biomineralization in an uncultivated multicellular magnetotactic prokaryote. *Environmental Microbiology Reports*, *6*(5), 524–531. https://doi.org/10.1111/1758-2229.12198

Kolinko, S., Richter, M., Glöckner, F. O., Brachmann, A., & Schüler, D. (2016). Single-cell genomics of uncultivated deep-branching magnetotactic bacteria reveals a conserved set of magnetosome genes. *Environmental Microbiology*, *18*(1), 21–37. https://doi.org/10.1111/1462-2920.12907

Komeili, A. (2012). Molecular mechanisms of compartmentalization and biomineralization in magnetotactic bacteria. *FEMS Microbiology Reviews*, *36*(1), 232–255. https://doi.org/10.1111/J.1574-6976.2011.00315.X

Kopp, R. E., & Kirschvink, J. L. (2008). The identification and biogeochemical interpretation of fossil magnetotactic bacteria. *Earth-Science Reviews*, *86*(1–4), 42–61. https://doi.org/10.1016/j.earscirev.2007.08.001

Körnig, A., Winklhofer, M., Baumgartner, J., Gonzalez, T. P., Fratzl, P., & Faivre, D. (2014). Magnetite crystal orientation in magnetosome chains. *Advanced Functional Materials*, *24*(25), 3926–3932. https://doi.org/10.1002/adfm.201303737

Koziaeva, V., Dziuba, M., Leão, P., Uzun, M., Krutkina, M., & Grouzdev, D. (2019). Genome-based metabolic reconstruction of a novel uncultivated freshwater magnetotactic coccus "Ca. Magnetaquicoccus inordinatus" UR-1, and proposal of a candidate family "Ca. Magnetaquicoccaceae". *Frontiers in Microbiology*, *10*, 2290. https://doi.org/10.3389/fmicb.2019.02290

Larrasoaña, J. C., Liu, Q. S., Hu, P. X., Roberts, A. P., Mata, P., & Civis, J. (2014). Paleomagnetic and paleoenvironmental implications of magnetofossil occurrences in late Miocene marine sediments from the Guadalquivir Basin, SW Spain. *Frontiers in Microbiology*, *5*, 71. https://doi.org/10.3389/Fmicb.2014.00071

Leão, P., Le Nagard, L., Yuan, H., Cypriano, J., Da Silva-Neto, I., Bazylinski, D. A., et al. (2020). Magnetosome magnetite biomineralization in a flagellated protist: Evidence for an early evolutionary origin for magnetoreception in eukaryotes? *Environmental Microbiology*, *22*(4), 1495–1506. https://doi.org/10.1111/1462-2920.14711

Lefèvre, C. T., & Bazylinski, D. A. (2013). Ecology, diversity, and evolution of magnetotactic bacteria. *Microbiology and Molecular Biology Reviews*, *77*(3), 497–526. https://doi.org/10.1128/mmbr.00021-13

Lefèvre, C. T., Howse, P. A., Schmidt, M. L., Sabaty, M., Menguy, N., & Luther, G. W. (2016). Growth of magnetotactic sulfate-reducing bacteria in oxygen concentration gradient medium. *Environmental Microbiology Reports*, *8*(6), 1003–1015. https://doi.org/10.1111/1758-2229.12479

Lefèvre, C. T., Menguy, N., Abreu, F., Lins, U., Pósfai, M., & Prozorov, T. (2011). A cultured greigite-producing magnetotactic bacterium in a novel group of sulfate-reducing bacteria. *Science*, *334*(6063), 1720–1723. https://doi.org/10.1126/science.1212596

Lefèvre, C. T., Pósfai, M., Abreu, F., Lins, U., Frankel, R. B., & Bazylinski, D. A. (2011). Morphological features of elongated-anisotropic magnetosome crystals in magnetotactic bacteria of the Nitrospirae phylum and the Deltaproteobacteria class. *Earth and Planetary Science Letters*, *312*(1–2), 194–200. https://doi.org/10.1016/j.epsl.2011.10.003

Lefèvre, C. T., Trubitsyn, D., Abreu, F., Kolinko, S., de Almeida, L. G. P., & de Vasconcelos, A. T. R. (2013). Monophyletic origin of magnetotaxis and the first magnetosomes. *Environmental Microbiology*, *15*(8), 2267–2274. https://doi.org/10.1111/1462-2920.12097

Lefèvre, C. T., Trubitsyn, D., Abreu, F., Kolinko, S., Jogler, C., & de Almeida, L. G. P. (2013). Comparative genomic analysis of magnetotactic bacteria from the Deltaproteobacteria provides new insights into magnetite and greigite magnetosome genes required for magnetotaxis. *Environmental Microbiology*, *15*(10), 2712–2735. https://doi.org/10.1111/1462-2920.12128

Li, J. H., Benzerara, K., Bernard, S., & Beyssac, O. (2013). The link between biomineralization and fossilization of bacteria: Insights from field and experimental studies. *Chemical Geology*, *359*, 49–69. https://doi.org/10.1016/j.chemgeo.2013.09.013

Li, J. H., Ge, K. P., Pan, Y. X., Williams, W., Liu, Q. S., & Qin, H. F. (2013). A strong angular dependence of magnetic properties of magnetosome chains: Implications for rock magnetism and paleomagnetism. *Geochemistry, Geophysics, Geosystems*, *14*, 3887–3907. https://doi.org/10.1002/Ggge.20228

Li, J. H., Menguy, N., Arrio, M. A., Sainctavit, P., Juhin, A., & Wang, Y. Z. (2016). Controlled cobalt doping in the spinel structure of magnetosome magnetite: New evidences from element- and site-specific X-ray magnetic circular dichroism analyses. *Journal of the Royal Society Interface*, *13*(121), 20160355. https://doi.org/10.1098/rsif.2016.0355

Li, J. H., Menguy, N., Gatel, C., Boureau, V., Snoeck, E., & Patriarche, G. (2015). Crystal growth of bullet-shaped magnetite in magnetotactic bacteria of the Nitrospirae phylum. *Journal of the Royal Society Interface*, *12*(103), 20141288. https://doi.org/10.1098/rsif.2014.1288

Li, J. H., Pan, Y., Liu, Q., Yu-Zhang, K., Menguy, N., Che, R., et al. (2010). Biomineralization, crystallography and magnetic properties of bullet-shaped magnetite magnetosomes in giant rod magnetotactic bacteria. *Earth and Planetary Science Letters*, *293*(3–4), 368–376. https://doi.org/10.1016/j.epsl.2010.03.007

Li, J. H., & Pan, Y. X. (2012). Environmental factors affect magnetite magnetosome synthesis in *Magnetospirillum magneticum* AMB-1: Implications for biologically controlled mineralization. *Geomicrobiology Journal*, *29*(4), 362–373. https://doi.org/10.1080/01490451.2011.565401

Li, J. H., Pan, Y. X., Chen, G. J., Liu, Q. S., Tian, L. X., & Lin, W. (2009). Magnetite magnetosome and fragmental chain formation of *Magnetospirillum magneticum* AMB-1: Transmission electron microscopy and magnetic observations. *Geophysical Journal International*, *177*(1), 33–42. https://doi.org/10.1111/j.1365-246X.2009.04043.x

Li, J. H., Zhang, H., Liu, P. Y., Menguy, N., Roberts, A. P., & Chen, H. T. (2019). Phylogenetic and structural identification of a novel magnetotactic Deltaproteobacterium strain WYHR-1 from a freshwater lake. *Applied and Environmental Microbiology*, *85*, e00731. https://doi.org/10.1128/aem.00731-19

Li, J. H., Zhang, H., Menguy, N., Benzerara, K., Wang, F. X., & Lin, X. T. (2017). Single-cell resolution of uncultured magnetotactic bacteria via fluorescence-coupled electron microscopy. *Applied and Environmental Microbiology*, *83*(12), 409–417. https://doi.org/10.1128/aem.00409-17

Lin, W., Bazylinski, D. A., Xiao, T., Wu, L. F., & Pan, Y. X. (2014). Life with compass: Diversity and biogeography of magnetotactic bacteria. *Environmental Microbiology*, *16*(9), 2646–2658. https://doi.org/10.1111/1462-2920.12313

Lin, W., Deng, A., Wang, Z., Li, Y., Wen, T., & Wu, L. F. (2014). Genomic insights into the uncultured genus "*Candidatus* Magnetobacterium" in the phylum *Nitrospirae*. *The ISME Journal*, *8*(12), 2463–2477. https://doi.org/10.1038/ismej.2014.94

Lin, W., Paterson, G. A., Zhu, Q., Wang, Y., Kopylova, E., & Li, Y. (2017). Origin of microbial biomineralization and magnetotaxis during the Archean. *Proceedings of the National Academy of Sciences, USA*, *114*(9), 2171–2176. https://doi.org/10.1073/pnas.1614654114

Lin, W., Zhang, W., Zhao, X., Roberts, A. P., Paterson, G. A., & Bazylinski, D. A. (2018). Genomic expansion of magnetotactic bacteria reveals an early common origin of magnetotaxis with lineage-specific evolution. *The ISME Journal*, *12*(6), 1508–1519. https://doi.org/10.1038/s41396-018-0098-9

Mann, S., Frankel, R. B., & Blakemore, R. P. (1984). Structure, morphology and crystal growth of bacterial magnetite. *Nature*, *310*(5976), 405–407. https://doi.org/10.1038/310405a0

Mann, S., Sparks, N. H. C., & Blakemore, R. P. (1987). Structure, morphology and crystal growth of anisotropic magnetite crystals in magnetotactic bacteria. *Proceedings of the Royal Society of London B*, *231*(1265), 477–487. https://doi.org/10.1098/rspb.1987.0056

Mao, X., Egli, R., Petersen, N., Hanzlik, M., & Liu, X. (2014). Magneto-chemotaxis in sediment: First insights. *PLoS ONE*, *9*, e102810. https://doi.org/10.1371/journal.pone.0102810

Meldrum, F. C., Mann, S., Heywood, B. R., Frankel, R. B., & Bazylinski, D. A. (1993a). Electron microscopy study of magnetosomes in a cultured coccoid magnetotactic bacterium. *Proceedings of the Royal Society of London B*, *251*(1332), 231–236. https://doi.org/10.1098/rspb.1993.0034

Meldrum, F. C., Mann, S., Heywood, B. R., Frankel, R. B., & Bazylinski, D. A. (1993b). Electron microscopy study of magnetosomes in two cultured vibrioid magnetotactic bacteria. *Proceedings of the Royal Society of London B*, *251*(1332), 237–242. https://doi.org/10.1098/rspb.1993.0035

Moskowitz, B. M., Frankel, R. B., & Bazylinski, D. A. (1993). Rock magnetic criteria for the detection of biogenic magnetite. *Earth and Planetary Science Letters*, *120*(3–4), 283–300. https://doi.org/10.1016/0012-821X(93)90245-5

Murat, D., Quinlan, A., Vali, H., & Komeili, A. (2010). Comprehensive genetic dissection of the magnetosome gene island reveals the step-wise assembly of a prokaryotic organelle. *Proceedings of the National Academy of Sciences, USA*, *107*(12), 5593–5598. https://doi.org/10.1073/pnas.0914439107

Olszewska-Widdrat, A., Schiro, G., Reichel, V. E., & Faivre, D. (2019). Reducing conditions favor magnetosome production in *Magnetospirillum magneticum* AMB-1. *Frontiers in Microbiology*, *10*, 582. https://doi.org/10.3389/fmicb.2019.00582

Pósfai, M., Kasama, T., & Dunin-Borkowski, R. E. (2013). Biominerals at the nanoscale: Transmission electron microscopy methods for studying the special properties of biominerals. *European Mineralogical Union Notes in Mineralogy*, *14*, 377–435. https://doi.org/10.1180/EMU-notes.14.11

Pósfai, M., Lefèvre, C., Trubitsyn, D., Bazylinski, D. A., & Frankel, R. B. (2013). Phylogenetic significance of composition and crystal morphology of magnetosome minerals. *Frontiers in Microbiology*, *4*, 344. https://doi.org/10.3389/fmicb.2013.00344

Pósfai, M., Moskowitz, B. M., Arató, B., Schüler, D., Flies, C., & Bazylinski, D. A. (2006). Properties of intracellular magnetite crystals produced by *Desulfovibrio magneticus* strain RS-1. *Earth and Planetary Science Letters*, *249*(3–4), 444–455. https://doi.org/10.1016/j.epsl.2006.06.036

Qian, X. X., Liu, J., Menguy, N., Li, J., Alberto, F., & Teng, Z. J. (2019). Identification of novel species of marine magnetotactic bacteria affiliated with Nitrospirae phylum. *Environmental Microbiology Reports*, *11*(4), 615–615. https://doi.org/10.1111/1758-2229.12777

Qian, X. X., Santini, C. L., Kosta, A., Menguy, N., Le Guenno, H., & Zhang, W. Y. (2020). Juxtaposed membranes underpin cellular adhesion and display unilateral cell division of multicellular magnetotactic prokaryotes. *Environmental Microbiology*, *22*(4), 1481–1494. https://doi.org/10.1111/1462-2920.14710

Rauch, E. F., Véron, M., Portillo, J., Bultreys, D., Maniette, Y., & Nicolopoulos, S. (2008). Automatic crystal orientation and phase mapping in TEM by precession diffraction. *Microscopy and Analysis*, *98*(6), 1–9. https://doi.org/10.1016/j.matchar.2014.08.010

Roberts, A. P., Chang, L., Heslop, D., Florindo, F., & Larrasoaña, J. C. (2012). Searching for single domain magnetite in the "pseudo-single-domain" sedimentary haystack: Implications of biogenic magnetite preservation for sediment magnetism and relative paleointensity determinations. *Journal of Geophysical Research*, *117*, B08104. https://doi.org/10.1029/2012JB009412

Roberts, A. P., Florindo, F., Villa, G., Chang, L., Jovane, L., & Bohaty, S. M. (2011). Magnetotactic bacterial abundance in pelagic marine environments is limited by organic carbon flux and availability of dissolved iron. *Earth and Planetary Science Letters*, *310*(3–4), 441–452. https://doi.org/10.1016/j.epsl.2011.08.011

Sparks, N. H. C., Mann, S., Bazylinski, D. A., Lovely, D. R., Jannasch, H. W., & Frankel, R. B. (1990). Structure and morphology of magnetite anaerobically-produced by a marine magnetotactic bacterium and a dissimilatory iron-reducing bacterium. *Earth and Planetary Science Letters*, *98*(1), 14–22. https://doi.org/10.1016/0012-821x(90)90084-b

Toro-Nahuelpan, M., Giacomelli, G., Raschdorf, O., Borg, S., Plitzko, J. M., & Bramkamp, M. (2019). MamY is a membrane-bound protein that aligns magnetosomes and the motility axis of helical magnetotactic bacteria. *Nature Microbiology*, *4*(11), 1978–1989. https://doi.org/10.1038/s41564-019-0512-8

Torres de Araujo, F. F., Pires, M. A., Frankel, R. B., & Bicudo, C. E. M. (1986). Magnetite and magnetotaxis in algae. *Biophysical Journal*, *50*(2), 375–378. https://doi.org/10.1016/S0006-3495(86)83471-3

Uebe, R., & Schüler, D. (2016). Magnetosome biogenesis in magnetotactic bacteria. *Nature Reviews Microbiology*, *14*(10), 621–637. https://doi.org/10.1038/nrmicro.2016.99

Usui, Y., Yamazaki, T., & Saitoh, M. (2017). Changing abundance of magnetofossil morphologies in pelagic red clay around Minamitorishima, Western North Pacific. *Geochemistry, Geophysics, Geosystems*, *18*, 4558–4572. https://doi.org/10.1002/2017GC007127

Yamazaki, T., Suzuki, Y., Kouduka, M., & Kawamura, N. (2019). Dependence of bacterial magnetosome morphology on chemical conditions in deep-sea sediments. *Earth and Planetary Science Letters*, *513*, 135–143. https://doi.org/10.1016/j.epsl.2019.02.015

Zhang, H., Menguy, N., Wang, F., Benzerara, K., Leroy, E., & Liu, P. (2017). Magnetotactic coccus strain SHHC-1 affiliated to Alphaproteobacteria forms octahedral magnetite magnetosomes. *Frontiers in Microbiology*, *8*, 969. https://doi.org/10.3389/fmicb.2017.00969

Zhou, K., Zhang, W. Y., Zhang, K. Y., Pan, H. M., Zhang, S. D., & Zhang, W. J. (2012). A novel genus of multicellular magnetotactic prokaryotes from the Yellow Sea. *Environmental Microbiology*, *14*(2), 405–413. https://doi.org/10.1111/j.1462-2920.2011.02590.x

Zhu, X., Hitchcock, A. P., Bazylinski, D. A., Denes, P., Joseph, J., Lins, U., et al. (2016). Measuring spectroscopy and magnetism of extracted and intracellular magnetosomes using soft X-ray ptychography. *Proceedings of the National Academy of Sciences, USA*, *113*(51), E8219–E8227. https://doi.org/10.1073/pnas.1610260114